Journal of Alloys and Compounds 509 (2011) 3661–3666

Contents lists available at ScienceDirect

Journal of Alloys and Compounds

journal homepage: www.elsevier.com/locate/jallcom

Optimization of transparent conducting oxide ZnO compound thickness in terms of four alloys thermo-physical performance aggregates

A. Amlouk[a], K. Boubaker[a,*], M. Bouhafs[b], M. Amlouk[a]

[a] Equipe de Physique des dispositifs à Semiconducteurs, Faculté des Sciences de Tunis, Campus Universitaire 2092 Tunis, Tunisia
[b] Unité de recherche MA2I, Ecole Nationale d'ingénieurs, ENIT, BP 37, Le Belvédère, Tunis, Tunisia

ARTICLE INFO

Article history:
Received 7 December 2010
Received in revised form
16 December 2010
Accepted 19 December 2010
Available online 28 December 2010

PACS:
73.61.Le
78.66.Li
79.60.Dp
61.10.Nz
68 .55.Jk

Keywords:
ZnO
Amlouk–Boubaker Opto-thermal expansivity ψ_{AB}
Transparent conducting oxides
Boubaker Polynomials Expansion Scheme
Micro-hardness
Optimization

ABSTRACT

ZnO is one of the well-known metal oxide semiconductors, which has been found, in the last four decades, to be very useful as transparent conductors and UV detectors in optoelectronic devices. This binary compound that showed quantum confinement effects in accessible size ranges was elaborated using several techniques. In the present work, the sprayed pyrolysis technique was carried out to prepare undoped ZnO crystals with different controlled thicknesses.

Particularly, and parallel to recently performed measurements, a recently proposed range of optimal layer thickness *d* is validated, through original conjoint morphological–structural–physical investigations.

1. Introduction

Transparent conducting oxides (TCO) have been recently investigated [1–6] for their interesting optical, mechanical and electrical performance. The lastly recorded [7–11] high optical transparence in the visible domain, and low electrical resistivity [12–17], led to numerous applications of these materials in the new generation of opto-electric devices [7–20].

Due to the ever decreasing scale of electronic devices using these transparent conducting oxides (TCO), there has been a growing interest in producing self-assembled micro-and nano-structured materials. Zinc oxide (ZnO) represents, in this context, an important basic material for the construction of nano-scale structures. Due to its low cost as well as its favorable opto-electronic and electro-luminescent properties, it has been satisfactorily implemented in acoustic devices [21], fluid sensors [22], transparent electrodes [23], and solar cells [24–28].

Commonly, these oxides could be synthesized using several methods [29,15,30–41] like reactive evaporation, electron beam evaporation (EBE), pulsed laser deposition (PLD), chemical vapor deposition (CVD), sol–gel coating, and chemical spray pyrolysis.

In this study, ZnO thin films have been prepared by spray pyrolysis technique using, as main precursor, a solution of zinc acetate dissolved in de-ionized water. Several characterization techniques such as XRD, optical spectra and hardness investigations have been applied to differently thick obtained samples [42–45]. The thickness-dependent performance of the different as-grown layers has been additionally investigated in terms of mechanical, opto-thermal and micro-hardness behaviours. The existence of an optimal thickness was discussed in comparison with some recently published results [46].

2. Experiment

2.1. Chemical kinetics of ZnO layers growth

ZnO thin layers have been prepared by the technique of chemical reactive technique in liquid phase spray. The obtained layers'

* Corresponding author.
E-mail address: boubaker_karem@yahoo.com (K. Boubaker).

0925-8388/$ – see front matter © 2010 Elsevier B.V. All rights reserved.
doi:10.1016/j.jallcom.2010.12.154

structural and morphological properties, as well as synthesizing details, have been recently published [42–45].

ZnO thin films having different thicknesses were obtained on $20 \times 10 \times 3\,mm^3$ Pyrex glass substrates by spraying an aqueous solution (mixture of water and propanol 2) containing zinc acetate ($Zn(CH_3CO_2)_2$) and a small amount of acetic acid, in order to avoid the precipitation of zinc hydroxide $Zn(OH)_2$. The solution and gas flow rates were kept constant at $2\,cm^3\,min^{-1}$ and $4.0\,l\,min^{-1}$ respectively corresponding to a mini-spray pyrolysis. The substrate temperature T_s, of the order of 460 °C (optimal value under the given experimental conditions, as already confirmed by Amlouk et al. [42,43]), was used to prepare these films according to in-room precedent successful attempts of deposition by the spray pyrolysis process [47,48].

The chemical process leading to an adherent ZnO film consists of three steps:

Step A: the droplets of zinc acetate ($Zn(CH_3CO_2)_2$ (ZA)) are dissociated under the effect of the heat:

$$\underset{\text{(droplets)}}{(Zn(CH_3CO_2)_2)_4} \xrightarrow[\text{acetic acid}]{\text{temperature}} \underset{\text{(gas,beyond substrate)}}{4\,Zn(CH_3CO_2)_2} \qquad \text{(Step A)}$$

Step B: the basic zinc acetate ($Zn_4O(CH_3COO)_6$ (BZA)) is produced by sublimation of the gaseous zinc acetate (ZA), and is instantaneously adsorbed at the substrate surface:

$$\underset{\text{(Gas, beyond substrate)}}{4\,Zn(CH_3CO_2)_2} + H_2O \xrightarrow{\text{Temperature}} \underset{\substack{\text{(Adsorbed)}\\ \text{(at substrate surface)}}}{Zn_4O(CH_3CO_2)_6} + \underset{\text{(Gas, beyond substrate)}}{2\,CH_3COOH}\uparrow$$

(Step B)

Step C: the basic zinc acetate ($Zn_4O(CH_3COO)_6$ (BZA)) yields the zinc oxide ZnO over the substrate surface:

$$\underset{\text{(Adsorbed)}}{Zn_4O(CH_3CO_2)_6} + 3\,H_2O \longrightarrow \underset{\text{(Solid, deposit)}}{4\,ZnO}\downarrow + \underset{\text{(Gas)}}{6\,CH_3COOH}\uparrow$$

(Step C)

The advantage of proceeding in a wet medium is illustrated, as noted earlier by Mar et al. [49], Paraguay et al. [50] and Khan and O'Brien [51], by the reduction of the amount of the residual carbon in the growing layer during the steps (B) and (C).

According to the monitored parameters, six samples have been elaborated: Z1, Z2, Z3, Z4, Z5 and Z6, with thicknesses $d = 0.16$, 0.4, 0.58, 0.64, 0.84 and 1.03 μm respectively.

2.2. Characterization techniques

The X-ray diffraction analysis of the prepared layers was performed by a copper-source diffractometer (Analytical X Pert PROMPD), with the wavelength ($\lambda = 1.54056$ Å). The optical transmission and reflection measures have been achieved using a common spectrophotometer (Shimadzu UV 3100S) equipped with an integrating sphere (LISR 3200). The spectrophotometer consists of double-beam monochromator with enough energy to make several types of accurate measures in a wide wave-length range (220–1800 nm). The morphological investigation along with hardness measurements have been performed in the *MA2I* Laboratory (ENIT, Tunis, Tunisia). The tests consisted of hitting the targeted face of each sample by a particularly flat diamond–pyramidal-indenter under a prefixed load. The obtained imprint dimensions were subjected to geometrical standardized analysis yielding a scaled value: the micro-hardness Vickers (Hv).

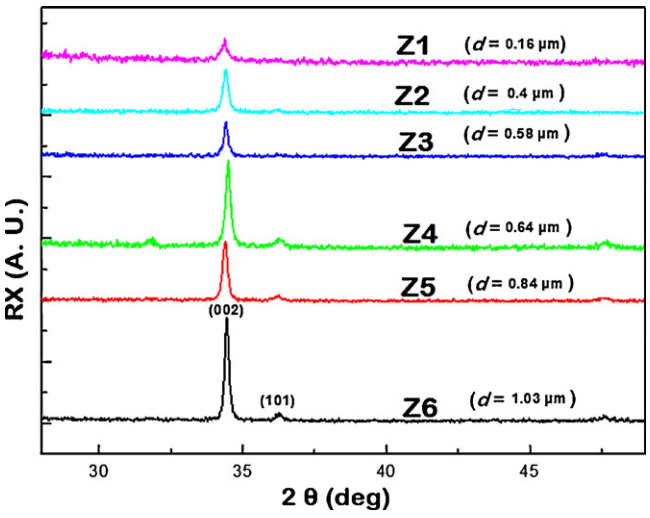

Fig. 1. XRD diagrams (ZnO layers $d = 0.16$, 0.4, 0.58, 0.64, 0.84 and 1.03 μm).

3. Results and discussion

3.1. X-ray diffraction investigations

XRD patterns of the deposited ZnO layers are shown in Fig. 1.

Diagram analysis (Fig. 1) shows that the thinner layers (Z1, Z2 and Z3) develop an exclusive preferred orientation of the crystallites with respect to the (0 0 2) reflection. Differently, the thicker ones, namely Z4, Z5 and Z6, are identified, beyond the (0 0 2) peak, by two extra XRD peaks: (1 0 1) and (1 0 0). This disposition corresponds to the hexagonal würtzite system (JCPDS card, file no.: 361451 <$a = 3.24982$, $c = 5.20661$Å>), which is generally associated, as stated by Lucio-Lopez et al. [52], Ratheesh Kumar et al. [53] and Paraguay et al. [54], with the appearance of irregularly spaced pores. This structure results in low transparency along with an increasing level of surface roughness.

Parallel to the XRD analyses, the FWHM data provided by XRD apparatus, were used to calculate and estimate the crystallite thickness D using Debye–Scherrer [55] formula:

$$D = \frac{K\lambda}{\beta \cos\theta} \qquad (1)$$

where $\lambda = 1.5418$ Å for Cu radiation, θ is the diffraction angle, $K = 0.9$, and β is the FWHM with $\beta = \sqrt{\beta_e^2 - \beta_0^2}$, where β_e is measured from the film and β_0 corresponds to the reference powder [55,56]. This formula allowed estimating average sizes of crystallites up to 200 nm.

It can be seen from the results summarized in Table 1, that for all these films, the crystallites are thinner than 200 nm, which shows the good crystalline quality of the films.

3.2. Optical properties

3.2.1. Optical transmission and reflection spectra

Figs. 2 and 3 show the optical transmission $T(\lambda)$ and reflection $R(\lambda)$ spectra, respectively, in the range (200–1800 nm).

Table 1
Crystallites thickness.

Sample	Z1	Z2	Z3	Z4	Z5	Z6
Crystallites thickness D (nm)	45.55	43.77	43.31	51.02	37.13	37.97

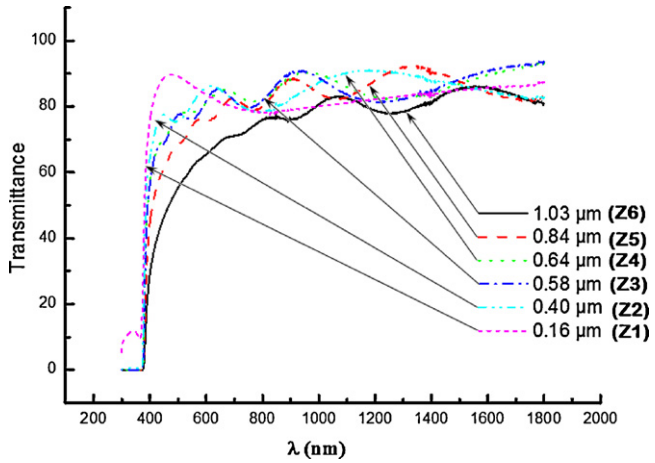

Fig. 2. Transmission spectra $T(\lambda)$.

Analysis of the obtained spectra and spectral lines data revealed that the six investigated samples are highly transparent in the visible near infrared domain ($T \approx 85\%$).

3.2.2. Films' thickness monitoring

The reflection $R(\lambda)$ spectra presented an accurate guide for estimating the thickness of each sample. In fact, the oscillating behaviour of the λ-dependent reflection in the visible domain (Fig. 3, label (A)), traduces the fact that the reflectance reaches discrete p-indexed maximal values $R^{(p)}_{max}$ for some particular p-indexed values λ^{p}_{max} of the wavelength [57–60].

These p-occurrences are traduced by the system:

$$\begin{cases} \sqrt{R^{(p)}_{max}(\lambda)} = \dfrac{n(\lambda^{p}_{max})^2 - n_S}{n(\lambda^{p}_{max})^2 + n_S} \\ n(\lambda^{p}_{max}) = \sqrt{n_S \dfrac{1+\sqrt{R_{max}(\lambda)}}{1-\sqrt{R_{max}(\lambda)}}} \end{cases} \quad (2)$$

Table 2
Samples thickness.

Sample	Z1	Z2	Z3	Z4	Z5	Z6
Thickness d (μm)	0.16	0.40	0.58	0.64	0.84	1.03

where n_s is the substrate optical index ($n_s \approx 1.55$) and n is the layer λ-dependent optical index deduced from the optical transmission-reflection spectra.

The knowledge of two successive couples of maximal values [58–60] allows calculating the film's thickness d:

$$d = \frac{\lambda^{p}_{max}\lambda^{p+1}_{max}}{2(\lambda^{p}_{max}n(\lambda^{p+1}_{max}) - \lambda^{p+1}_{max}n(\lambda^{p}_{max}))} \quad (3)$$

The calculated values of the thickness d are gathered in Table 2.

3.3. Mechanical micro-hardness Vickers (Hv) investigations

The micro-hardness Vickers (Hv) set of measurements has been performed using a common diamond–pyramidal-indenter under a prefixed load. The obtained imprint dimensions have been exploited for yielding the micro-hardness Vickers (Hv) of each sample as a synthetic value. The obtained values are gathered in Fig. 4.

The differences noticed in Fig. 4 can be explained, for the layers (Z1, Z2, Z3 and Z4), by the hardness contribution of the Pyrex substrate. The remaining layers, namely Z5 and Z6, develop a mean hardness varying in a narrow interval. If the contribution of the substrate can be omitted, it seems that there is a maximum hardness zone situated in the interval of thickness [0.70–0.80 μm].This feature is in perfect concordance with precedent observations (Section 3.1).

3.4. Opto-thermal study

3.4.1. Determination of the effective absorptivity $\hat{\alpha}$ using the BPES

The effective absorptivity $\hat{\alpha}$, as defined in precedent studies [61,62], is the mean normalized absorbance weighted by $I(\tilde{\lambda})_{AM1.5}$,

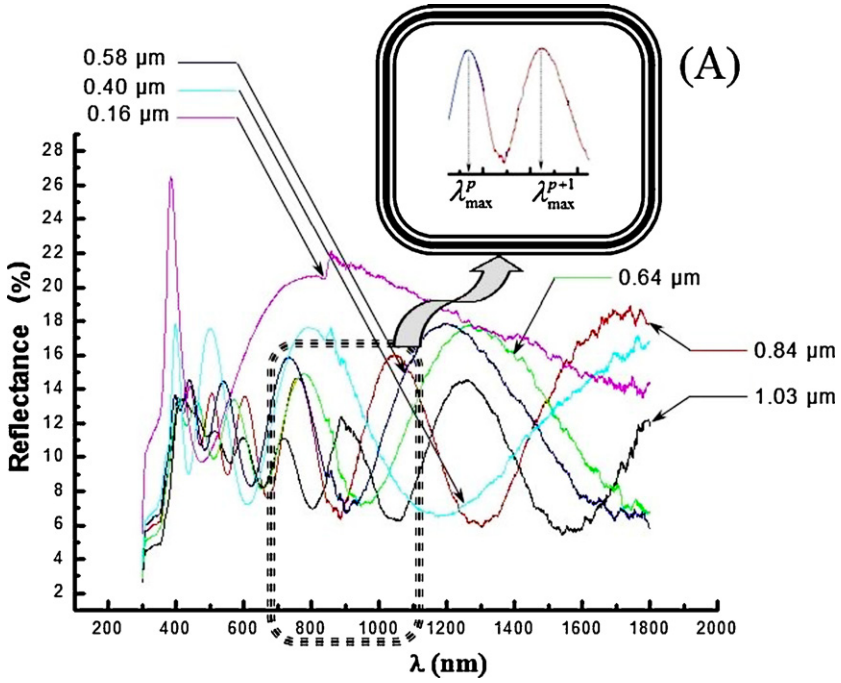

Fig. 3. Reflection spectra $R(\lambda)$.

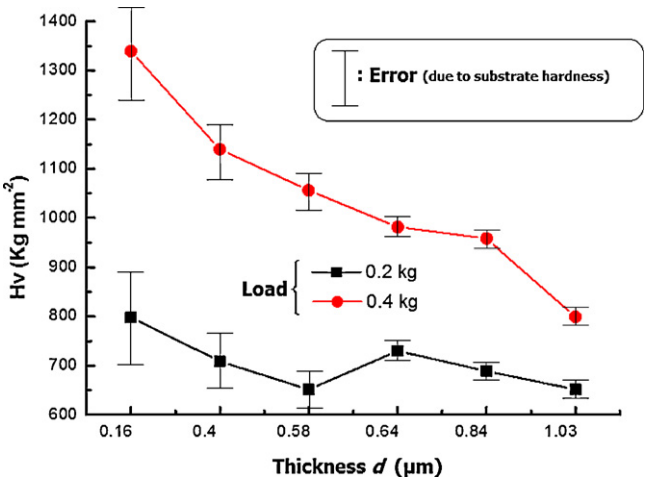

Fig. 4. The micro-hardness Vickers (Hv) measurements.

the solar standard irradiance:

$$\hat{\alpha} = \frac{\int_0^1 I(\tilde{\lambda})_{\mathrm{AM1.5}} \times \alpha(\tilde{\lambda}) d\tilde{\lambda}}{\int_0^1 I(\tilde{\lambda})_{\mathrm{AM1.5}} d\tilde{\lambda}} \tag{4}$$

where $I(\tilde{\lambda})_{\mathrm{AM1.5}}$ is the reference solar spectral irradiance, fitted using the Boubaker Polynomials Expansion Scheme (BPES) [63–77]: $I(\tilde{\lambda}) = [(1/2N_0)\sum_{n=1}^{N_0} \theta_n \cdot B_{4n}(\tilde{\lambda} \times \beta_n)]$, where β_n are the Boubaker polynomials [65–69] B_{4n} minimal positive roots, θ_n are given coefficients, N_0 is a given integer, $\alpha(\tilde{\lambda})$ is the normalized absorbance spectrum and $\tilde{\lambda}$ is the normalized wavelength:

$$\begin{cases} \lambda \in [\lambda_{\min}, \lambda_{\max}] \Leftrightarrow \tilde{\lambda} \in [0, 1] \\ \lambda_{\min} = 300.0\,\mathrm{nm};\ \lambda_{\max} = 1800.0\,\mathrm{nm} \end{cases} \tag{5}$$

The normalized absorbance spectrum $\alpha(\tilde{\lambda})$ is deduced from the BPES by establishing a set of N experimental measured values of the transmittance–reflectance vector $(T_i(\tilde{\lambda}_i); R_i(\tilde{\lambda}_i))|_{i=1..N}$ versus the normalized wavelength $\tilde{\lambda}_i|_{i=1..N}$. Then the system (6) is set:

$$\begin{cases} R(\tilde{\lambda}) = \left[\dfrac{1}{2N_0}\displaystyle\sum_{n=1}^{N_0} \xi_n \times B_{4n}(\tilde{\lambda} \times \beta_n)\right] \\ T(\tilde{\lambda}) = \left[\dfrac{1}{2N_0}\displaystyle\sum_{n=1}^{N_0} \xi'_n \times B_{4n}(\tilde{\lambda} \times \beta_n)\right] \end{cases} \tag{6}$$

where β_n are the 4n-Boubaker polynomials B_{4n} minimal positive roots [68,71], N_0 is a given integer and ξ_n and ξ'_n are coefficients determined through the Boubaker Polynomials Expansion Scheme (BPES).

The normalized absorbance spectrum $\alpha(\tilde{\lambda})$ is deuced from the relation:

$$\alpha(\tilde{\lambda}) = \frac{1}{d\sqrt[4]{2}} \cdot \sqrt[4]{\left(\ln\frac{1-R(\tilde{\lambda})}{T(\tilde{\lambda})}\right)^4 + \left(2\ln\frac{1-R(\tilde{\lambda})}{\sqrt{T(\tilde{\lambda})}}\right)^4} \tag{7}$$

where d is the layer thickness.

The obtained value of normalized absorbance spectrum $\alpha(\tilde{\lambda})$ is a final guide to the determination of the effective absorptivity $\hat{\alpha}$ through (Eq. (4)).

Table 3
Values of the Amlouk–Boubaker opto-thermal expansivity ψ_{AB}.

Sample	Z1	Z2	Z3	Z4	Z5	Z6
ψ_{AB} (10^{-12} m^3 s^{-1})	25.22	22.80	12.32	10.12	15.43	18.22

3.4.2. Determination of Amlouk–Boubaker opto-thermal expansivity ψ_{AB}

The Amlouk–Boubaker opto-thermal expansivity ψ_{AB} is a thermo-physical parameter defined in precedent studies [61–68], as a 3D expansion velocity of the transmitted heat inside the material. It is expressed in m^3 s^{-1}, and calculated by:

$$\psi_{AB} = \frac{D}{\hat{\alpha}} \tag{8}$$

where D is the thermal diffusivity and $\hat{\alpha}$ is the effective absorptivity (Section 3.4.1).

The values of the calculated values of the Amlouk–Boubaker opto-thermal expansivity ψ_{AB}, for the different samples, are gathered in Table 3.

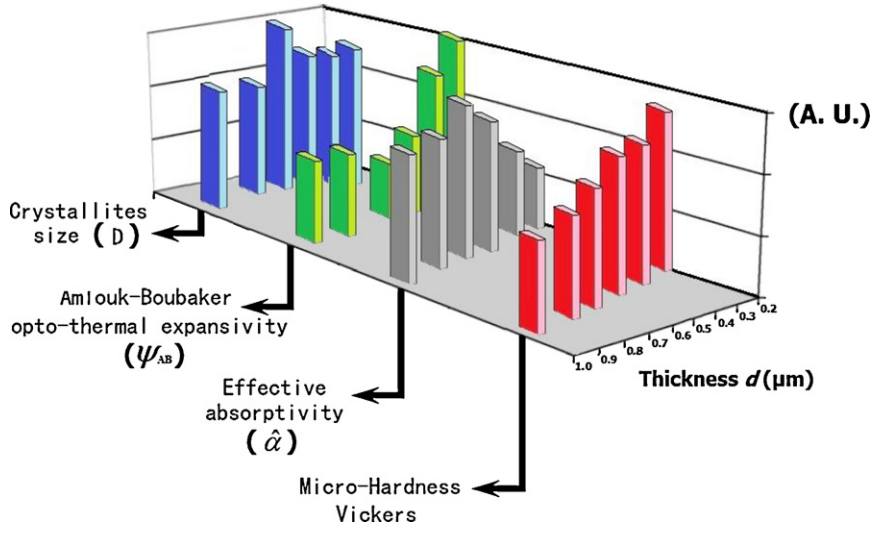

Fig. 5. Global optimality abacus gathering four optimizing-decisive parameters: crystallite size, opto-thermal expansivity, effective absorptivity and hardness.

4. Discussion and perspectives

A very instructive study has been recently presented by Lee et al. [78] on the thickness-related optimization inside IZO/ZnO/PET multi-layerd structures. The authors have prospected the ZnO-induced exclusive electrical performance (carriers' concentration, mobility, . . .) and conjectured the existence of an eventual optimal thickness. Earlier, Shan Lee et al. [79] attempted to verify optimality for a thickness around 500 nm. These intriguing observations allowed suggesting the existence of a similar optimality in the case of ZnO monolayered structure. In fact, it has been sustainably proposed that two main conditions have to be ensured in order to obtain good performance of ZnO sprayed thin films for TCO applications:

- A *good transparency* (which is closely related to the orientation of crystallites along the axis perpendicular to *c* axis plane of the substrate as well as a higher value on their size).
- A *low value* of $\psi_{\mathbf{AB}}$, *the Amlouk–Boubaker opto-thermal expansivity*, a parameter that indicates and brings together a low thermal diffusivity (hence low heat loss) of zinc oxide layer with a high absorption coefficient which attests better its use for TCO applications.

For this purpose, a conjoint evaluation of several performance indicators (opto-thermal constants, crystallites size, etc.) has been achieved on the basis of a 3D abacus (Fig. 5). A thorough analysis of the conjoint variation versus thickness confirms the conjectured [46] and never demonstrated layered ZnO thin films thickness.

Moreover, the mechanical study revealed that, in order to reach the intrinsic hardness value of the layer (required for TCO applications in shock circumstances or aggressive mediums, . . .), while avoiding substrate effects, one must either use a load as low as possible, or ensure a thickness exceeding the micrometer. Still, these values can be refined by using the nano-hardness measurements to obtain the accurate hardness values of such thin films.

5. Conclusion

In summary, we have discussed the effects of the controlled thickness of ZnO thin films prepared using a simplified and already optimized spray pyrolysis setup. Besides commonly considered parameters of the obtained layers, like bandgap, roughness, and transparency, new and original characterization protocols have been carried out. It has been stated that an optimal ZnO thin film thickness is required for TCO purposes via simultaneous morphological–structural–physical investigations. Nano-hardness investigations along with prospecting the theoretical dependence of the thickness versus the amount of the precursor material are programmed.

References

[1] M. Regragui, V. Jousseaume, M. Addou, A. Outzourhit, J.C. Bernéde, B. El Idrissi, Thin Solid Films 397 (2001) 238–243.
[2] F. Yubero, V.M. Jiménez, A.R. Gonzalez-Elipe, Surf. Sci. 400 (1998) 116–126.
[3] E. G-Berasategui, S.J. Bull, T.F. Page, Thin Solid Films 447–448 (2004) 26–32.
[4] R. Thokala, J. Chaudhuri, Thin Solid Films 266 (1995) 189–191.
[5] R.B. Patil, R.K. Puri, V. Puri, J. Alloys Compd. 462 (2008) 235–239.
[6] P.M. Gorley, V.V. Khomyak, S.V. Bilichuk, I.G. Orletsky, P.P. Horley, V.O. Grechko, Mater. Sci. Eng. B 118 (2005) 160–163.
[7] D. Davazoglu, A. Donnadieu, Thin Solid Films 147 (1987) 131–142.
[8] S.W. Xue, X.T. Zu, W.L. Zhou, H.X. Deng, X. Xiang, L. Zhang, H. Deng, J. Alloys Compd. 448 (2008) 21–26.
[9] T. Serin, N. Serin, S. Karadeniz, H. Sarı, N. Tugluoglu, O. Pakma, J. Non-Cryst. Solids 352 (2006) 209–215.
[10] D. Souri, K. Shomalian, J. Non-Cryst. Solids 355 (2009) 1597–1608.
[11] J.C. Manifacier, Thin Solid Films 90 (1982) 297–308.
[12] A. Mosbah, T.A. Moustaghfir, S. Abed, N. Bouhssira, M.S. Aida, E. Tomasella, M. Jacquet, Surf. Coat. Technol. 200 (2005) 293–296.
[13] Y. Villachon-Renard, G. Levèque, A. Abdellaoui, A. Donnadieu, Thin Solid Films 203 (1991) 33–39.
[14] N. Kikuchi, E. Kusano, E. Kishio, A. Kinbara, Vacuum 66 (2002) 365–371.
[15] G.X. Liu, F.K. Shan, W.J. Lee, B.C. Shin, H.S. Kim, J.H. Kim, Ceram. Int. 34 (2008) 1011–1015.
[16] E. Elangovan, K. Ramamurthi, J. Optoelectron. Adv. Mater. 5 (2003) 45–52.
[17] L. Niinistö, J. Päiväsaari, J. Niinistö, M. Putkonen, M. Nieminen, Phys. Stat. Sol. (a) 201 (7) (2004) 1443–1452.
[18] K. Ramamoorthy, M. Jayachandran, K. Sankaranarayanan, P. Misra, L.M. Kukreja, C. Sanjeeviraja, Curr. Appl. Phys. 4 (2004) 679–684.
[19] H.-C. Cheng, C.-F. Chen, C.-C. Lee, Thin Solid Films 498 (2006) 142–145.
[20] Y. Furubayashi, T. Hitosugi, Y. Yamamoto, Y. Hirose, G. Kinoda, K. Inaba, T. Shimada, T. Hasegawa, Thin Solid Films 496 (2006) 157–159.
[21] W. Water, S.-Y. Chu, Y.-D. Juang, S.-J. Wu, Mater. Lett. 57 (2002) 998–1004.
[22] M. Suchea, S. Chiritoulakis, K. Moschovis, N. Katsarakis, G. Kiriakidis, Thin Solid Films 515 (2006) 551–566.
[23] F. Michlotti, A. Belardini, A. Rousseau, A. Ratsimihety, G. Schoer, J. Mueller, J. Non-Cryst. Solids 352 (2006) 2339–2344.
[24] J. Hupkes, B. Rech, O. Kluth, T. Repmann, B. Zwayagardt, J. Muller, R. Drese, M. Wutting, Sol. Energy Mater. Sol. Cells 90 (2006) 3054–3066.
[25] S. Nagae, M. Toda, M. Minemoto, H. Takakura, Y. Hamakawa, Sol. Energy Mater. Sol. Cells 90 (2006) 3568–3575.
[26] N. Phuangpornpitak, S. Kumar, Renew. Sust. Energy Rev. 1 (2007) 1530–1543.
[27] S. Rehman, I.M. El-Amin, F. Ahmad, S.M. Shaahid, A.M. Al-Shehri, J.M. Akhashwain, A. Shash, Renew. Sust. Energy Rev. 11 (2007) 635–653.
[28] W.J. Jeong, S.K. Kim, G.C. Park, Thin Solid Films 506–507 (2006) 180–199.
[29] X.Q. Wei, J.Z. Huang, M.Y. Zhang, Y. Du, B.Y. Man, Mater. Sci. Eng. B 166 (2010) 141–146.
[30] H. Hallil, P. Ménini, H. Aubert, Procedia Chem. 1 (2009) 935–938.
[31] J. Bandara, C.M. Divarathne, S.D. Nanayakkara, Sol. Energy Mater. Sol. Cells 81 (2004) 429–437.
[32] A. Alkaya, R. Kaplan, H. Canbolat, S.S. Hegedus, Renew. Energy 34 (2009) 1595–1599.
[33] K.-W. Kim, P.-S. Cho, S.-J. Kim, J.-H. Lee, C.-Y. Kang, J.-S. Kim, S.-J. Yoon, Sens. Actuators B 123 (2007) 318–324.
[34] G. Leo, R. Rella, P. Siciliano, S. Capone, J.C. Alonso, V. Pankov, A. Ortiz, Sens. Actuators B 58 (1999) 370–374.
[35] J. Montero, J. Herrero, C. Guillén, Sol. Energy Mater. Sol. Cells 94 (2010) 612–616.
[36] T. Prasada Rao, M.C. Santhoshkumar, Appl. Surf. Sci. 255 (2009) 4579–4584.
[37] T. Ratana, P. Amornpitoksuk, T. Ratana, S. Suwanboon, J. Alloys Compd. 470 (2009) 408–412.
[38] A.F. Khan, M.r. Mehmood, M. Aslam, M. Ashraf, Appl. Surf. Sci. 256 (2010) 2252–2258.
[39] E. Senadım, S. Eker, H. Kavak, R. Esen, Solid State Commun. 139 (2006) 479–484.
[40] J. Szuber, G. Czempik, R. Larciprete, B. Adamowicz, Sens. Actuators B 70 (2000) 177–181.
[41] J.-H. Chung, Y.-S. Choe, D.-S. Kim, Thin Solid Films 349 (1999) 126–129.
[42] A. Amlouk, K. Boubaker, M. Amlouk, J. Alloys Compd. 490 (2010) 602–604.
[43] A. Amlouk, K. Boubaker, M. Amlouk, M. Bouhafs, J. Alloys Compd. 485 (2009) 887–891.
[44] S. Dabbous, T. Ben Nasrallah, J. Ouerfelli, K. Boubaker, M. Amlouk, S. Belgacem, J. Alloys Compd. 487 (2009) 286–292.
[45] B. Ouni, J. Ouerfelli, A. Amlouk, K. Boubaker, M. Amlouk, J. Non-Cryst. Solids 356 (2010) 1294–1299.
[46] K. Boubaker, Mat. Sci. Eng. A MSEA, in press.
[47] M. Amlouk, S. Belgacem, N. Kamoun, H. EL Houichet, R. Bennaceur, Semicond. Thin Films, Ann. Chim. Fr. 19 (1994) 469–477.
[48] M. Amlouk, F. Touhari, S. Belgacem, N. Kamoun, D. Barjon, R. Bennaceur, Phys. Stat. Sol. (a) 163 (1997) 73–84.
[49] G.L. Mar, P.Y. Timbrell, R.N. Lamb, Chem. Mater. 5 (1995) 7–14.
[50] F. Paraguay, W. Estrada, D.R. Acosta, E. Andrade, M. Miki-Yoshida, Thin Solid Films 350 (1999) 192–202.
[51] O.F.Z. Khan, P. O'Brien, Thin Solid Films 173 (1989) 95–104.
[52] M.A. Lucio-Lopez, M.A. Luna-Arias, A. Maldonado, M. de la, L. Olvera, D.R. Acosta, Sol. Energy Mater. Sol. Cells 90 (2006) 733–741.
[53] P.M. Ratheesh Kumar, S. Kartha, K.P. Vijayakumar, J. Appl. Phys. 98 (2005) 023509–23516.
[54] F. Paraguay, D.J. Morales, W. Estrada, L.E. Andrade, M. Miki-Yoshida, Thin Solid Films 366 (2000) 16–21.
[55] B.D. Cullity, Elements of X-ray Diffraction, A.W. Pub. Comp. Inc., 1978.
[56] E.F. Kaeble, Handbook of X-rays, McGraw-Hill, New York, 1967.
[57] S. Belgacem, J.M. Saurel, J. Bougnot, Thin Solid Films 92 (1982) 199–206.
[58] S. Belgacem, R. Bennaceur, J. Saurel, J. Bougnot, Rev. Phys. Appl. 25 (1990) 1245–1258.
[59] D.A. Minkov, J. Phys. D 22 (1989) 199–207.
[60] R. Swanepoel, J. Phys. E 16 (1983) 1214–1222.
[61] S. Lazzez, K.B. Ben Mahmoud, S. Abroug, F. Saadallah, M. Amlouk, Curr. Appl. Phys. 9 (2009) 1129–1134.
[62] K.B. Ben Mahmoud, M. Amlouk, Mater. Lett. 63 (2009) 991–999.
[63] S. Slama, M. Bouhafs, K.B. Ben Mahmoud, Int. J. Heat Technol. 26 (2008) 141–152.
[64] B. Dubey, T.G. Zhao, M. Jonsson, H. Rahmanov, J. Theor. Biol. 264 (2010) 154–160.
[65] D.H. Zhang, F.W. Li, Ir. J. Appl. Phys. Lett. 2 (2009) 25–33.
[66] O.B. Awojoyogbe, K. Boubaker, Curr. Appl. Phys. 9 (2009) 278–288.
[67] J. Ghanouchi, H. Labiadh, K. Boubaker, Int. J. Heat Technol. 26 (2008) 49–57.

[68] K.B. Ben Mahmoud, J. Thermophys. Heat Transfer 23 (2009) 409–421.
[69] T.G. Zhao, Z.S. Wang, K.B. Ben Mahmoud, Int. J. Math. Comp. 1 (2008) 13–20.
[70] T.G. Zhao, L. Naing, W.X. Yue, Mat. Zametki. 87 (2) (2010) 175–178.
[71] K. Boubaker, Numer. Methods Part. Diff. Equat. 25 (2009) 802–811.
[72] A. Yildirim, S.T. Mohyud-Din, D.H. Zhang, Comp. Math. Appl. 59 (2010) 2473–2488.
[73] A. Belhadj, J. Bessrour, M. Bouhafs, L. Barrallier, J. Therm. Anal. Calorim. 97 (2009) 911–922.
[74] S. Tabatabaei, T. Zhao, O. Awojoyogbe, F. Moses, Heat Mass Transfer 45 (2009) 1247–1252.
[75] S. Fridjine, M. Amlouk, Mod. Phys. Lett. B 23 (2009) 2179–2188.
[76] O.D. Oyodum, O.B. Awojoyogbe, M. Dada, J. Magnuson, Eur. Phys. J. Appl. Phys. 46 (2009) 21201–21211.
[77] A. Belhadj, O. Onyango, N. Rozibaeva, J. Thermophys. Heat Transfer 23 (2009) 639–653.
[78] C. Lee, A. Park, Y. Cho, M. Park, W. Lee, H.W. Kim, Ceram. Int. 34 (2008) 1093–1096.
[79] F.K. Shan Lee, Y.S. Yu, J. Eur. Ceram. Soc. 24 (2004) 1869–1872.